LANGMUIR

Interface Components: Nanoparticles, Colloids, Emulsions, Surfactants, Proteins, Polymers

Preparation of Colloidally Stable Positively Charged Hollow Silica Nanoparticles: Effect of Minimizing Hydrolysis on Zeta Potentials

Hyunho Kang, Davis J. Long, and Christy L. Haynes

Langmuir, **Just Accepted Manuscript** • Publication Date (Web): 22 May 2019

Preparation of Colloidally Stable Positively Charged Hollow Silica Nanoparticles: Effect of Minimizing Hydrolysis on Zeta Potentials

*Hyunho Kang, Davis J. Long, and Christy L. Haynes**

Department of Chemistry, University of Minnesota, 207 Pleasant Street SE, Minneapolis, MN 55455, United States

*Corresponding author, chaynes@umn.edu

Abstract

Silica nanoparticles have received great attention as versatile nanomaterials in many fields such as drug delivery, sensing, and imaging due to their physical and chemical flexibility. Specifically, the silanol groups at the surface of silica nanoparticles have enabled various surface modifications and functionalization to tailor the nanoparticles for each application. Chemical tailoring to switch from negative to positive surface charge has been one important strategy to enhance cell internalization and biodistribution of the nanoparticles. However, efficient surface charge modification that is sustained upon dispersion is difficult to achieve and has not been well characterized, though it can be a critical requirement for successful nanoparticle performance. In this study, solid spherical silica nanoparticles and hollow spherical silica nanoparticles around 45 nm in diameters were synthesized, both possessing tunable positive zeta potentials in aqueous colloidal suspension, to investigate the relationship between time-dependent zeta potential changes and their morphologies. The set of three different particles showing varied zeta

potentials of approximately 5 mV, 20 mV, and > 30 mV in both morphologies were prepared, and their colloidal surface electric potential fluctuations were measured. These studies reveal that the hollow morphologies are much more effectively able to maintain positive zeta potentials for seven days of aqueous incubation, whereas the magnitude of the zeta potential of the solid silica spheres decreases uncontrollably, largely due to hydrolysis of the interior siloxane bonds, resulting in adsorption of the released silicic acid onto the nanoparticle surface.

Introduction

Silica-based nanomaterials have been extensively studied and advanced in recent years, and a variety of industrial fields are using silica nanomaterials for various purposes. For example, silica-based nanosols play a crucial role in inks and coatings where many functional applications have been commercialized for anticorrosion and antimicrobial applications.[1] Organically modified silica materials enable efficient selective hydrogenation of oils[2] or aerobic oxidation of alcohols.[3] Silica nanocomposites with polymers or metal nanoparticles have a diverse range of applications in catalysis,[4] optics,[5] and the automotive industry.[6] Furthermore, in biomedical research, silica nanoparticles have been heavily studied as drug delivery cargo agents,[7] sensors,[8] and imaging nanocomposites.[9] The form of the silica nanoparticles may take solid, mesoporous, hollow, or core-shell morphologies.[5] The size of the nanoparticles is generally tunable during synthesis for any of these morphologies. Combined with tunable size and morphology, the biocompatibility, low toxicity, and synthetic scalability of the silica nanoparticles have made them excellent candidates for a variety of bio-related applications. For example, Gao et al. recently demonstrated the application of mesoporous silica shell-coated iron oxide nanoparticles in cryopreservation to enable rewarming of vitrified tissues.[10]

The synthetic flexibility with silica nanoparticles can be largely attributed to the development of two major synthesis strategies: gas-phase synthesis and liquid-phase synthesis.[11] Due to the significantly lower energy cost and simpler required apparatus, liquid-phase synthesis is the more common approach in most research fields. Sol-gel and microemulsion syntheses, where the nanoparticles are produced through the condensation polymerization of silica precursor molecules, are most popular. Depending on the synthetic pH, temperature, precursor concentration, and other added chemicals, the final nanoparticle product can display various sizes, morphologies, porosities, and surface areas.

Among the different types of colloidal silica nanoparticles, one universal property is the functionalizable silanol groups at the surface of the nanoparticles, where alkoxysilanes can covalently modify the surface via hydrolysis-condensation polymerization. These silanes grant the nanoparticle platform useful properties; for example, modification with (3-aminopropyl)trimethoxysilane facilitates further modification with inking moieties such as n-hydroxysuccinide-functionalized molecules, isothiocynates, malemides, etc.[12] Also common, various polyethylene glycol silanes allow for enhanced colloidal stability via steric repulsion.[13] In addition, thiol-silane-functionalized porous silica nanoparticles can react with polymers to form a hybrid, enabling temperature-controlled uptake and release of small molecules from within their mesopores.[14]

Display of a positive zeta potential in colloidal suspension is another important factor for nanoparticles to function properly, especially during biological cell-nanoparticle interactions. Thus, many studies have worked to understand and improve nanoparticle-cell interactions via silane surface functionalization. In 2008, Yang and co-workers developed trimethylammonium-silane functionalized mesoporous silica nanoparticles for loading and release of anionic drug molecules.[15] Upon pH change in the environment around the nanoparticles, the drugs loaded via electrostatic attraction were released due to deprotonation of the silanol groups. Shahabi et al. studied the effect of surface charge and the presence of serum on nanoparticle uptake by human osteoblast cells by synthesizing solid silica nanoparticles with different zeta potentials.[16] The authors found that the character of the surface functionalization induced different interactions between the silica nanoparticles and the cells. The same researchers also investigated the influence of mesoporous silica nanoparticles with silane-based functionalization on the encapsulation and release of the anticancer drug doxorubicin as well as cancer cell response.[17] In this case, the nanoparticles were functionalized with sulfonate, polyethylene glycol, or polyethylene imine, and nanoparticles with cationic surface charges showed efficient uptake by cells. Wang and co-workers found that electrostatic interaction between positively charged silica nanoparticle and negatively charged cancer cells rendered much stronger and kinetically faster binding than was achieved via immunological interaction with antibody-functionalized magnetic silica nanoparticles.[18]

As such, it is clear that display of positive surface charge is critical for biological application of silica nanoparticles where cellular membrane-nanoparticle interaction and penetration is key to enhancing the nanomaterial performance. For this reason, surface modification has been applied to solid spherical nanoparticles, mesoporous silica, hollow silica, and multifunctional nanocomposites using a variety of methods.[19] However, the resultant zeta potentials vary between studies, and the prepared nanoparticles often display significant undesired polydispersity.[20] Though maintenance of this positive surface charge is critical, most studies haven't reported how long the nanoparticles maintain their positive zeta potential while in colloidal suspension. This maintenance of positive zeta potential may be particularly challenging for silica nanoparticles with their network of siloxane linkages and silanol groups. During colloidal dispersion in aqueous systems, silica nanoparticles are likely to be hydrolyzed, resulting in more silanol groups and an increasingly negative zeta potential. Further, maintenance of the electric potential can be an essential requisite in biomedical research where the colloidal stability must be maintained during blood circulation until approaching targeting sites.

The study reported in this paper started with a goal to prepare a series of silica nanoparticles possessing varied positive zeta potentials in aqueous-based media and to examine the influence of surface electric potentials on the interactions with cellular membranes and organism systems. During the nanoparticle preparation, it quickly became obvious that the prepared silica nanoparticles were not able to hold the intended zeta potentials for a long time following dispersion. As such, we realized that it was important to understand the cause of the nanoparticles' unsustained zeta potentials in colloidal suspension to enable a fabrication path to prepare positively-charged silica nanoparticles with consistent zeta potentials in aqueous media. We hypothesized that the maintenance of the silica nanoparticles' zeta potentials was closely related to morphology as the degree of condensation within the silica network should be dependent on bond depth within the nanostructure. In this study, we prepared surface-modified solid silica nanoparticles via reverse-micro emulsion. The surface of the silica nanoparticles was modified during or after the micro emulsion via condensation of a quaternary ammonium silane, and maintenance of zeta potential was investigated. We found that, even with successful surface modification, the solid silica still displayed a large possibility of losing the positive electric potentials during aqueous colloidal dispersion. Thus, to reveal the main cause of the declining positive zeta potentials or charge reversal, surface-functionalized hollow silica nanoparticles were prepared from solid silica nanoparticles as a dissolving template. In this synthesis, no external materials except silica nanoparticles and silanes are needed to produce hollow structures, where hydrolysis of the existing siloxane network and condensation of the introduced silane on the surface occur at the same time. The experimental results showed that the zeta potential changes in the colloidal dispersion were induced mainly by the adsorption of silicic acid originating from the dissolving inner regions of the solid silica, not from the loss of the functional silanes on the surface. An improved resistance to hydrolysis and to zeta potential change was achieved when the nanoparticles were tuned to have hollow structures and modified further with a hydrophobic silane at high temperature. Maintenance of the electric potential of the amorphous spherical silica nanoparticles in the colloidal state can be achieved when nanoparticles are synthesized to possess a high degree of condensation, as is the case with the hollow silica nanospheres. This research is expected to be beneficial for silica nanoparticle preparation in various fields, such as drug delivery and nanoparticle toxicity research, where the maintenance of the modified surface electric potential in colloidal state can be critical for the expected performance of the particles.

Experimental Section

Material Characterizations. *Transmission Electron Microscopy (TEM).* TEM images were taken with an FEI Tecnai T12 at 120 kV. The nanoparticles were dispersed in 99% ethanol, and Formvar/carbon-coated copper grids (Ted Pella, INC, Redding, CA) were dipped into the suspension to transfer the nanoparticles to the grids. The grids were then dried in air. For the nanoparticle aging in water, the samples were prepared the same way, but the grids were dried in air for 24 hours to prepare the sample.

Dynamic Light Scattering (DLS) and ζ-Potential Measurements. For hydrodynamic diameter measurements, a Brookhaven 90Plus particle analyzer (Holtsville, NY) equipped with a 35 mW red diode laser (660 nm) was used. The nanoparticles were dispersed in ultrapure water, and DLS was measured after at least 10 minutes of sonication for homogenous dispersion of the nanoparticles. Each value in this report consists of the average of three measurements, and the error bars in this report represent the standard deviations of the three measurements. The ζ-potential measurements were conducted with a Brookhaven ZetaPALS Zeta-Potential Analyzer (Holtsville, NY); the values were obtained from ten averaged runs, each consisting of ten cycles, and the error bars in this report represent the standard deviations of the ten averaged runs.

UV-Vis Extinction Measurements. UV-Vis extinction spectra were recorded using a DH-2000 light source (Oceans Optics, Largo, FL). During the surface-modified hollow silica nanoparticle preparation, extinction at 310 nm was measured before and after the TMAC addition at various time points. To measure the extinction from the silica nanoparticles accurately, the extinction from a 0.256 M NH_4OH solution with TMAC and without $sSiO_2$ was subtracted. The same experiment was performed without TMAC addition. Each value was averaged from three independent measurements and the error bars represent the standard deviations of the three measurements.

X-ray Photoelectron Spectroscopy Measurements. The surface elemental analysis of TMAC-modified $sSiO_2$ ($sSiO_2$_TMAC) were conducted via PHI 5000 Versa Probe III (Physical Electronics, Chanhassen, MN). Each nanoparticle was dried via rotary evaporator to remove ethanol. The ethanolic suspensions of particles were dried in scintillation vials with a rotary evaporator. The dried and powdered nanoparticles were transferred onto the sample holder using double-sided tape. For each sample, less than 2 mg was used for surface elemental analysis.

Surface Area Measurements. The surface areas of the solid and hollow silica nanoparticles were measured using Brunauer-Emmett-Teller (BET) analysis of nitrogen adsorption-desorption isotherms via Micromeritics ASAP 2020 system at 77K (Norcross, GA). Each dried and powdered sample was degassed at a pressure of 10 μm Hg at 120 °C for at least 24 hours before the measurement.

Discussion and Results

The original solid silica nanoparticles ($sSiO_2$) for these surface modification studies were synthesized via reverse-micro emulsion, with slight modifications from previous reports.[21] In this method, each emulsion acts as an individual micro reactor where a single silica nanoparticle is generated. The synthesized nanoparticles show monodisperse morphology and size based on TEM images, and their hydrodynamic diameters and zeta potentials were stable in pure water for 7 days or longer (Figure S1ab). Though mesoporous silica nanoparticles (MSNs) are of particular interest, this work makes use of solid silica because it is more straightforward to observe any changes induced following surface modification, such as changes in size or morphology. For example, when the primary amine silane (APTES) was added to MSNs, depending on the amount of the silane, the synthesized MSNs showed significant morphology changes (Figure S1cd).

The quaternary ammonium silane N-trimethoxysilylpropyl-N,N,N-trimethylammonium chloride (TMAC) was used in this work to imbue a positive surface charge, rather than the more typical APTES, since these quaternary ammonium cations are permanently charged and not affected by pH (Figure S2b). In our first attempt, TMAC was added during the reverse-micro emulsion state, but after the silica nanoparticles had already been generated inside the emulsion (Figure S2a). This was based on the initial speculation that TMAC would form a coating on the silica nanoparticles so that mono-disperse silica nanoparticles with quaternary ammonium groups on the surface would yield positively charged silica nanoparticles. However, as shown in TEM images, the silica nanoparticles showed a great degree of polydispersity, depending on the amounts of TMAC added (Figure S2cd). Also, even when an excess of TMAC was added, the zeta potentials were still not positive (data not shown). The reason for the enlarged silica nanoparticles is presumably due to Ostwald ripening.[23] In the reverse-micro emulsion, TritonX-100 and 1-hexanol serve as a soft shell which contain a water droplet surrounded by cyclohexane as an organic solvent. As hydrophobic TEOS is added, it dissolves into the organic solvent first. The ammonium hydroxide hydrolyzes TEOS to silicic acid (SiO_4^{4-}), the silicic acid moves into the water droplet, and condensation/nucleation generates the silica nanoparticles in the water droplet. This softly-confined nanoreactor space then experiences the coalescence kinetics which determine the nanoparticle size. When two emulsion droplets collide, they might fuse into a larger droplet or repulse each other. This force should be dependent on the surface energy of the droplets, which is affected by chemical composition, temperature, and solubility of the monomer in the two different phases.[6] The coalescence and fusion are likely to occur when the droplet needs to lower the surface energy. TMAC is innately amphiphilic and more likely to reside at the interface between the oil and water of the droplet.[24] In this case, TMAC might break the stable surface energy state defined by hexanol and TritonX-100, and the droplet collisions induce coalescence so that the smaller droplets fuse into the larger droplets to lower the surface energy, resulting in heterogeneous nanoparticle size.

To obtain monodisperse and effectively surface-modified silica nanoparticles, TMAC was added after the nanoparticles were prepared in a two-step nanoparticle preparation. The as-synthesized $sSiO_2$ nanoparticles were dried, and the powdered nanoparticles were redispersed in an ethanol/water mixture containing ammonium hydroxide along with TMAC in reflux (see SI for the detailed procedure). The amount of TMAC used was chosen based on estimation of the number of silanol groups on the surface to attain varied positive charges (see calculations in Additional Supporting Information and Table S1 and S2).[22] Figure S3a and b show representative TEM images of the nanoparticles without surface modification and those modified to display the highest positive zeta potentials. The surface-modified nanoparticles ($sSiO_2$_TMAC) show no observable morphology changes or diameter increments compared to the unmodified nanoparticles. Figure S3b shows the TEM image of the $sSiO_2$_TMAC, and from the image it is clear that the density of the modified solid nanoparticles is less than that of sSiO2 in Figure S3a, indicating that during the surface modification there was some hydrolysis of siloxane bonds and, thus, dissolution to silicic acid. We attempted to avoid this small change by refluxing the nanoparticles in an ethanol-only solution, but this did not allow for the necessary hydrolysis and condensation of TMAC. In Figure 1, the TEM diameters, the hydrodynamic diameters, and zeta potentials of four solid silica nanoparticles (an unmodified one and three surface-modified ones with varied zeta potentials via reflux in H_2O/EtOH mixture). It is clear that as the positive zeta potential values increased, the hydrodynamic diameters also decreased, even though TEM images indicated no significant differences among the four sets of primary nanoparticles. This indicates that the nanoparticles formed a flocculation when the electrostatic repulsion among nanoparticles were not sufficiently large to achieve colloidal stability. Thus, it is straightforward to reason that DLS measurements of the particles with low positive zeta potentials do not reveal the primary nanoparticle hydrodynamic size, but rather represents the size of agglomerates due to the insufficient electrostatic repulsion among particles. It is reasonable to speculate that both silanol groups and quaternary ammonium groups exist on the nanoparticle surface and that the varying ratio between the two groups cause different net charges upon colloidal dispersion.

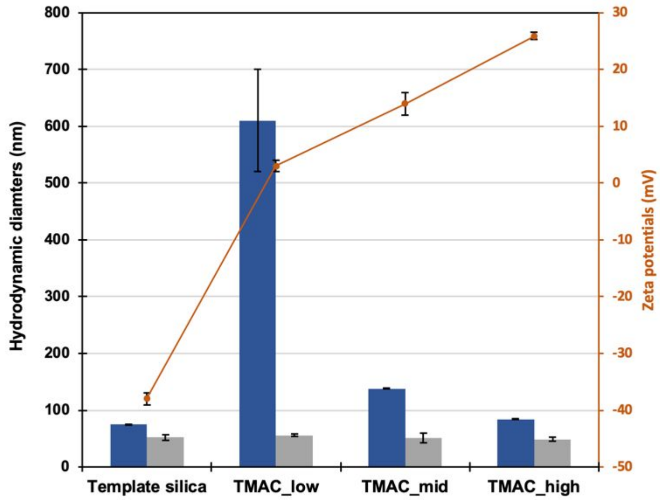

Figure 1. Hydrodynamic diameters of four different silica nanoparticles (blue); TEM diameters (n=300) of the four different silica nanoparticles (grey); and zeta potentials of four different silica nanoparticles in pure water (orange). The concentrations of the aqueous suspensions were 0.2 mg/mL for all nanoparticles.

The surface elemental compositions of the three nanoparticles with different positive zeta potentials were analyzed via XPS. In Figure 2a, from all nanoparticles except the unmodified nanoparticle ($sSiO_2$), nitrogen was detected along with oxygen, carbon, and silicon. In Figure S4, a high-resolution nitrogen XPS spectrum from the nanoparticles with the highest zeta potential ($sSiO_2$_TMAC_high) shows two peaks at 402.6 eV and 399.5 eV; these are attributed to cationic species and neutral species, respectively. From the nanoparticles, a very small amount of chloride ion has been detected, so it is likely that the neutralized quaternary ammonium nitrogen peak comes from the silanes with chloride ions still adsorbed. In Figure 2b, the atomic percentages of each element from each nanoparticle are provided. As the zeta potential increases, the percentages of nitrogen from the nanoparticles also increases. However, these percentage values were relative within each sample, and inter-nanoparticle comparisons may not be relevant because carbon contamination in environmental air may affect the measured values. Thus, we focused on the percentage ratios between Si and N in each sample as both elements should come only from the nanoparticles and TMAC. These data show that a higher ratio of N to Si gives rise to higher zeta potentials in colloidal suspensions, which confirms that higher TMAC surface coverage induces more surface electric potential reversal from negative to positive without significant change in the nanoparticles' physical properties in this two-step synthesis.

(a)

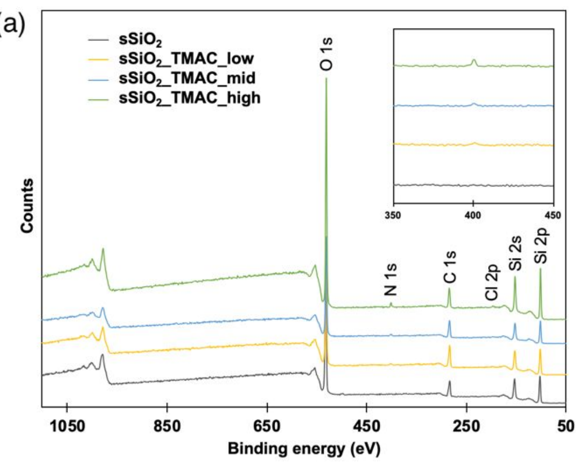

(b)

	$sSiO_2$	$sSiO_2$_TMAC_low	$sSiO_2$_TMAC_mid	$sSiO_2$_TMAC_high
O (%)	60.0	53.3	53.4	60.0
Si (%)	21.6	20.4	20.9	23.1
C (%)	18.4	25.3	24.1	14.6
N (%)	-	1.1	1.6	2.1
N/Si	-	0.054	0.077	0.09

Figure 2. (a) XPS spectra of four silica nanoparticles (template silica and $sSiO_2$_TMAC prepared from reflux with different amounts of TMAC). (b) XPS atomic percentage results from four silica nanoparticles (Template silica and $sSiO_2$_TMAC prepared from reflux in a water/ethanol mixture with different amounts of TMAC). The bottom row shows the atomic ratio between nitrogen and silicon from three $sSiO_2$_TMAC particles.

The nanoparticles ($sSiO_2$_TMAC) prepared by the two-step method were incubated for 24 hours in pure water, and the zeta potentials were measured every 8 hours to track their stabilities. However, the positive zeta potentials of the $sSiO_2$_TMAC kept decreasing during the incubation, and the zeta potential of $sSiO_2$_TMAC refluxed in ethanol only, which initially showed a negative potential, became more negative (Figure 3a). Figure 3b shows a TEM image of the $sSiO_2$_TMAC (refluxed in H_2O/EtOH) after 5 days of aqueous incubation. From the image, it is obvious that the interior regions of the nanoparticles have been changed more than the outer regions. Based on the changes in both the zeta potential and nanoparticle morphology, we hypothesized that the change in zeta potentials for the $sSiO_2$_TMAC is related to the dissolved and released silicic acid from the interior regions adsorbing onto the surface of the silica, rather than loss of the TMAC ligand. Several researchers have studied the degree of condensation of silica precursors located in different parts of the silica nanoparticle.[25–27] Generally, it is accepted that the core region of a silica sphere has a lower degree of condensation and are thus more likely to be hydrolyzed and dissolved when incubated in water (Scheme 1). Thus, we reasoned that the TMAC on the surface of the nanoparticle could remain even though the zeta potential decreased, as the charge from the TMAC is screened by the silicic acid, resulting in colloidal instability of the nanoparticles.

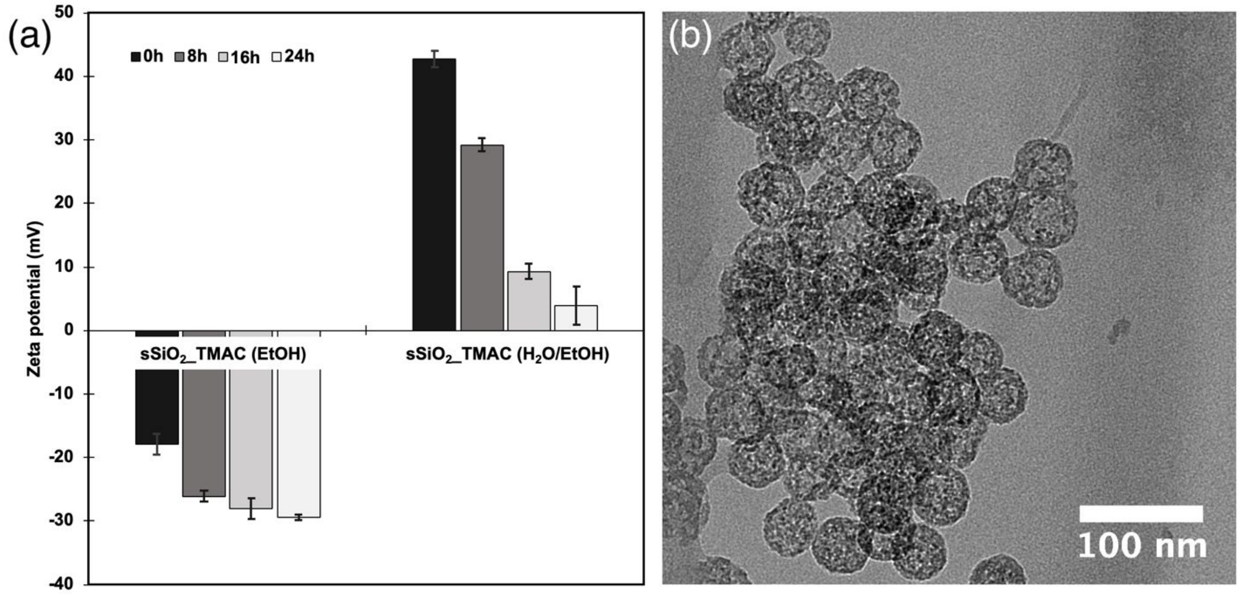

Figure 3. (a) Zeta potentials of $sSiO_2$_TMAC suspended in pure water for 24 hours. Reflux in two different conditions (in ethanol only and in water/ethanol mixture) were used to produce two different nanoparticles. (b) TEM image of $sSiO_2$_TMAC (H_2O/EtOH) after the nanoparticles were suspended in water for 5 days.

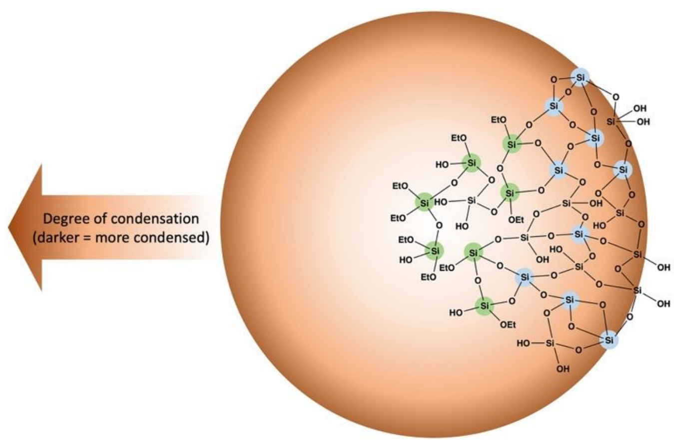

Scheme 1. Schematic description of the local degree of condensation of the amorphous silica spheres synthesized via reverse-micro emulsion. The silicon atoms highlighted in green possess the ethoxy groups which are not hydrolyzed from TEOS. The silicon atoms highlighted in blue show the fully condensed silicates. This schematic is not drawn to scale.

To estimate the relationship between the core region dissolution and zeta potential maintenance, another synthetic protocol was considered. The method (Figure 4a) uses as-synthesized $sSiO_2$ as a dissolving template to condense a newly introduced silane.

The goal of this synthesis was to condense TMAC on the surface and dissolve the weakly condensed silica precursors at the same time, generating a hollow structure with a greater overall percentage of fully condensed silica (see SI for the detailed procedure). Different from the previously reported methods where a foreign template such as polystyrene bead needs to be calcined at a high temperature,[28,29] the as-synthesized solid silica template can be removed in the same solution without placing the nanoparticles in harsh conditions. The ammonium hydroxide solution with elevated temperature catalyzed both this hydrolysis and the condensation reaction, and TEM images (Figure 4b) clearly show the hollow structure of the final product ($hSiO_2$_TMAC). Nitrogen adsorption-desorption analysis was conducted to confirm the hollow structures, and the surface area increased by 176% due to the hollow shell formation (Figure 4c). The hollow silica nanoparticles show much less turbidity upon colloidal dispersion compared to the solid sphere at the same concentration (Figure S5). All these results indicate that, in a basic aqueous condition, the mixture of the silica template and the silane can produce hollow structures via simultaneous hydrolysis and condensation.

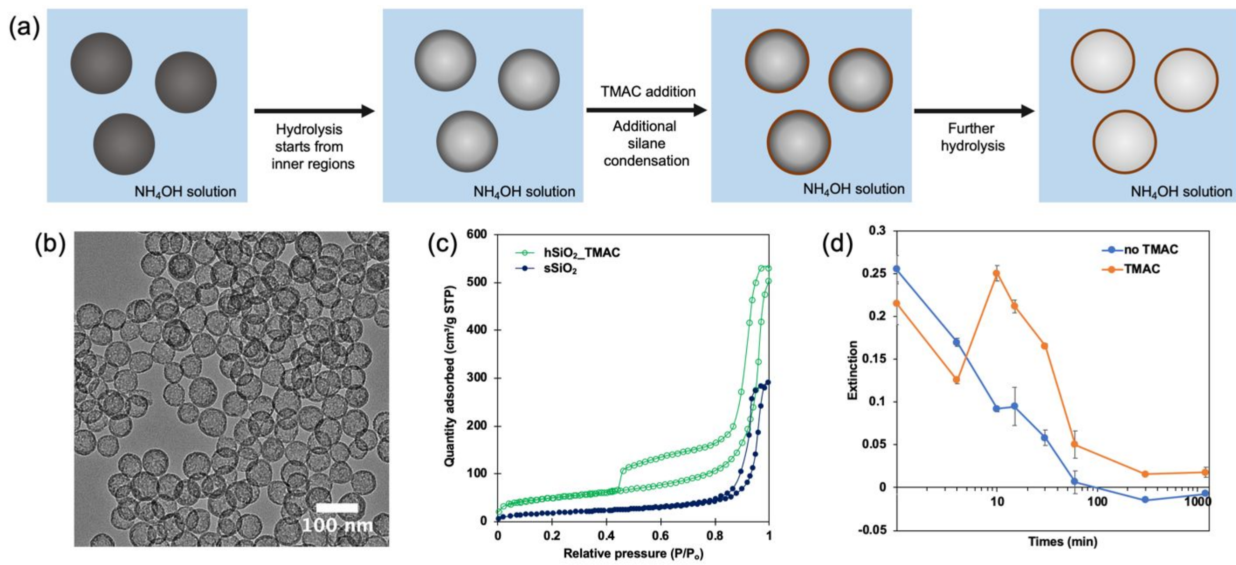

Figure 4. (a) Schematic description of hollow silica nanoparticle formation by using $sSiO_2$ as a dissolving template. (b) TEM image of the as-synthesized $hSiO_2$_TMAC. (c) Nitrogen adsorption-desorption plots, and (d) Time-dependent extinction (at 310 nm) of silica nanoparticle suspensions during hollow silica formation comparing when TMAC was absent (blue) and present (orange).

Dynamic observation of the transformation from the solid to the hollow structure was conducted via UV-Vis extinction spectra of the silica nanoparticle suspensions. The silica nanoparticles don't have a specific extinction wavelength, but a broad extinction in the range of 200 to 400 nm.[30] As shown in Figure 4d, the nanoparticles dispersed in NH_4OH solution without TMAC showed a gradual decrease in extinction optical density (OD) at 310 nm, and eventually the value went to zero, indicating that no nanoparticles remained. However, 5 minutes after TMAC addition, the nanoparticles with TMAC showed an abrupt OD increase (at 10 minutes in Figure 4d) due to the rapid hydrolysis and condensation of TMAC on the surface. After that, the OD decreased in the same manner the template solid silica had, but the value remained positive, reflecting the hollow silica nanoparticles still in suspension (Figure 4d). This observation reveals that the initial TMAC condensation on the surface of the nanoparticles is a critical factor for the hollow structure formation and preventing the complete dissolution of the template silica. This is not just the specific behavior of TMAC, the same trends were seen when PEG or TEOS were added instead, and the same hollow structures were obtained (Figure S6).

During hollow silica formation, several factors can affect the silica dissolution and the final morphology, including temperature, nanoparticle/silane concentration, and pH. We varied each parameter to evaluate its impact. Figure 5 shows the TEM images of the final nanoparticles synthesized in each condition. It is clear that the pH had little impact on the formation of hollow nanostructures; the same is true of the amount of TMAC as long as the NH_4OH solution volume was low (Figure 5ab). The most drastic morphological changes were found when the solution volume was large enough to dissolve the entire suspended silica nanoparticle. In these cases, the amount of TMAC added plays an important role in hollow structure formation. If the amount of TMAC is too high, hollow silica wasn't formed as uniformly or effectively as in the suspensions with the lower amounts of TMAC (Figure 5c). Also, if the template silica concentration was too low, even with excess TMAC, no hollow nanoparticles were formed (Figure 5d). Overall, this series of experiments showed that there are two critical factors determining the formation of hollow silica nanoparticles: (1) the amount of additional silane introduced and (2) the original solid silica template concentration. It is widely known that the hydrolysis and condensation of the alkoxysilane is strongly influenced by the ratio of water to silane and alkoxide, the nature of the R groups, and the types of catalysts.[31] In the synthesis process of the hollow silica nanoparticles, the molar amount of water versus the mass concentration of the silica template nanoparticles determines a final equilibrium state in regard to the hydrolysis, and thus dissolution of the nanoparticles. It is also well-known that the aqueous solubility of the amorphous silica nanoparticles involves an equilibrium between the colloidal nanoparticles and a monomeric or polymeric silicic acid.[32] It is generally thought that the monosilicic acid, presumably $Si(OH)_4$, is the most common product of silica dissolution. When it is assumed that the dissolved silicic acid doesn't change the pH, the equilibrium state is mainly governed by the water volume, pH, and temperature. Previous reports have shown that the effect of the pH on the final equilibrium state is not as strong as its effect on the rate of the dissolution.[33,34] Thus, the hollow structure wasn't formed when the water amount wasn't sufficient to dissolve the solid silica in Figure 5ab, regardless of the pH and amount of TMAC. When the water volumes reach a level where the suspended silica nanoparticles can be dissolved to a significant degree, the TMAC added afterwards seems to impact hollow structure formation by changing the equilibrium state. This newly introduced silane in the solution can delay dissolution and decrease the amount of released silicic acid from the nanoparticles by establishing a new equilibrium state. The hollow silica structure is attributed to the different degrees of condensation of the silica in different portions of the original solid silica template. Though it may seem to be counterintuitive that the inner regions of the silica nanoparticles are "softer" than outer regions, several studies have shown that the inner parts of the silica nanoparticles possess fewer fully condensed silicon atoms than the outer parts, resulting in harder and more compact cross-linking of silica on the surface.[35,36] It can thus be reasoned that during the synthesis, the hydrolysis and condensation of TEOS, the silica precursor, initiate the nucleation of the silica nanoparticles, and the core is where the condensation occurs at the beginning of the synthesis with nanoparticles growing as the condensation continues. Thus, the inner regions are more likely to have the partially hydrolyzed precursors and ethoxy groups

(OC_2H_5), making these parts softer and more susceptible to dissolution. The TMAC can support the hollow structure formation by not only establishing a new equilibrium state but also by acting as a protective layer on the surface, as in a previous report where PVP protected a silica surface against NaOH etching.[37] TMAC could increase the condensation degree at the surface by producing more siloxane bonds among silanol groups on the surface, resulting in a more dissolution-resistant silica surface. However, when the silica template concentration is much lower than the standard experimental condition, TMAC wasn't able to maintain the special structure of the original template, and it seems that TMAC barely retained the morphological vestige of the template nanoparticle or was hydrolyzed and condensed itself (Figure 5d). Thus, it is clear that carefully manipulated synthetic conditions can be exploited to dissolve the silica template and condense the silane simultaneously to produce hollow silica spheres.

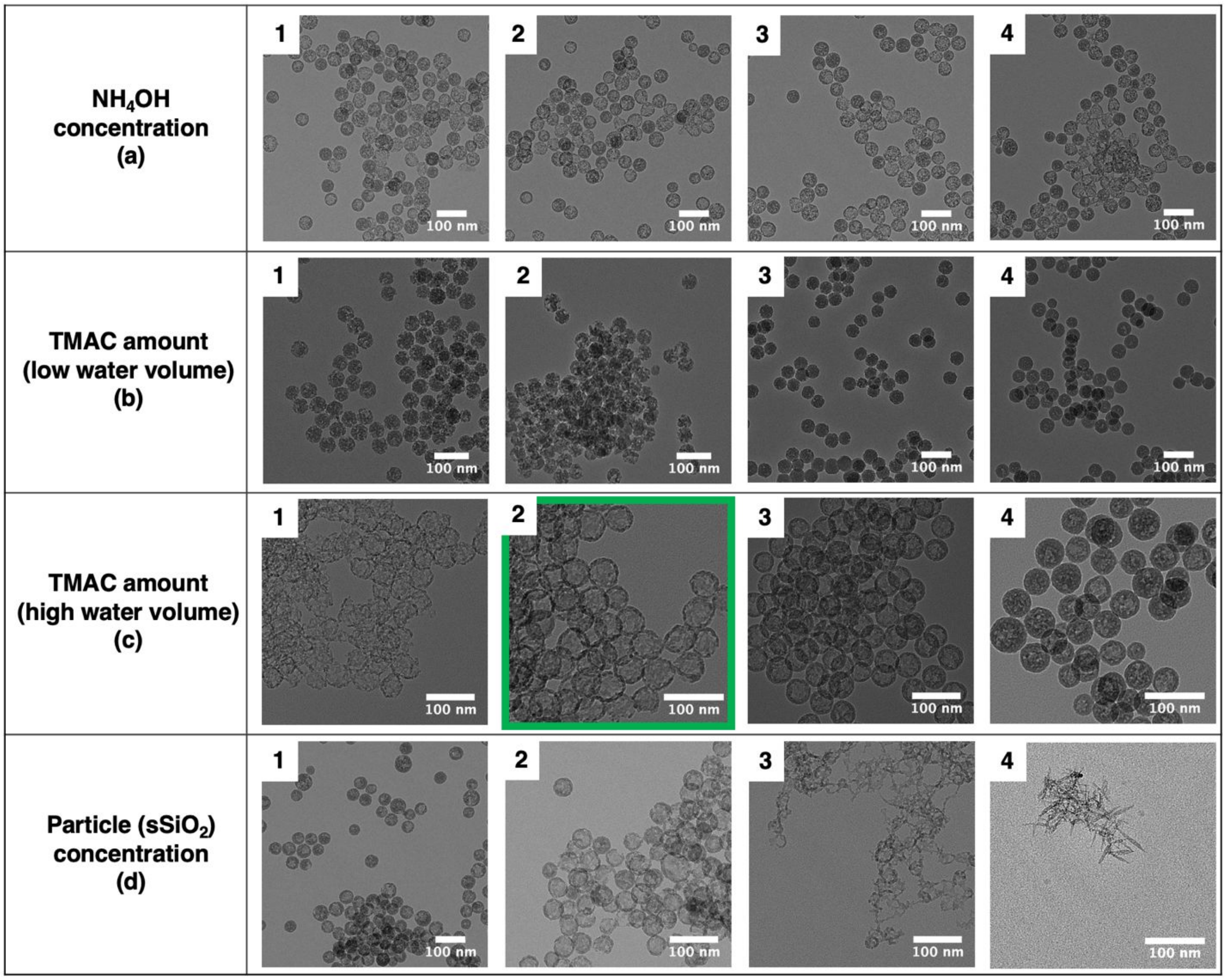

Figure 5. TEM images of the synthesized silica nanoparticles intended to produce hollow silica nanoparticles ($hSiO_2$_TMAC) in various conditions. The image in the green box (c-2) contains the $hSiO_2$_TMAC synthesized from the standard condition as described in the Methods section. Every other image includes the nanoparticles synthesized with modified parameters. For (a), the NH_4OH volumes were 15 mL for all samples and concentrations were tuned to (a-1) 0.128 M, (a-2) 0.256 M, (a-3) 0.384 M, and (a-4) 0.512 M. For (b), the NH_4OH volumes were 10 ml for all samples, and the volumes of the diluted TMAC were varied to (b-1) 10 μL, (b-2) 50 μL, (b-3) 100 μL and (b-4) 300 μL. For (c), the NH_4OH volumes were 15 mL for all samples, and the volumes of the diluted TMAC were varied to (c-1) 10 μL, (c-2) 100 μL, (c-3) 200 μL and (c-4) 300 μL. For (d), the volumes of the 20 mg/mL $sSiO_2$ ethanolic suspensions added were tuned to (d-1) 1.4 mL, (d-2) 1.2 mL, (d-3) 0.7 mL, (d-4) 0.35 mL. For (d-4), the volume of the diluted TMAC was an excess as well. All parameters not mentioned here explicitly were the same as in the standard condition introduced in SI.

The hollow structures, however, still present the zeta potential decrease shown in Figure 6. The solid silica with lower zeta potential, with higher zeta potential ($sSiO_2$_TMAC_low and $sSiO_2$_TMAC_high, respectively), and the hollow silica ($hSiO_2$_TMAC) all showed drops in the magnitude of their positive zeta potentials upon incubation in water, though the rate of the decrease was the slowest for the $hSiO_2$_TMAC (suggesting the effect of the particular morphology on maintaining the surface electric potentials). Interestingly, when all three nanoparticles were centrifuged and re-dispersed in pure water again, the initial zeta potentials recovered, reflecting that TMAC remained condensed on the surface, and the zeta potential changes had occurred due to the dissolved inner silica of the nanoparticles. For all three nanoparticles, especially the solid silica with lower zeta potential ($sSiO_2$_TMAC_low), higher zeta potentials than the previous values (Figure 1) were achieved. This occurred because the small degree of core region dissolution and charge screening due to the released silicic acid took place during the first incubation of powdered nanoparticles upon sonication. In the redispersion, this effect is weaker since the silica precursors which were the most susceptible to hydrolysis had already been released during the first dispersion and incubation, resulting in higher zeta potentials.

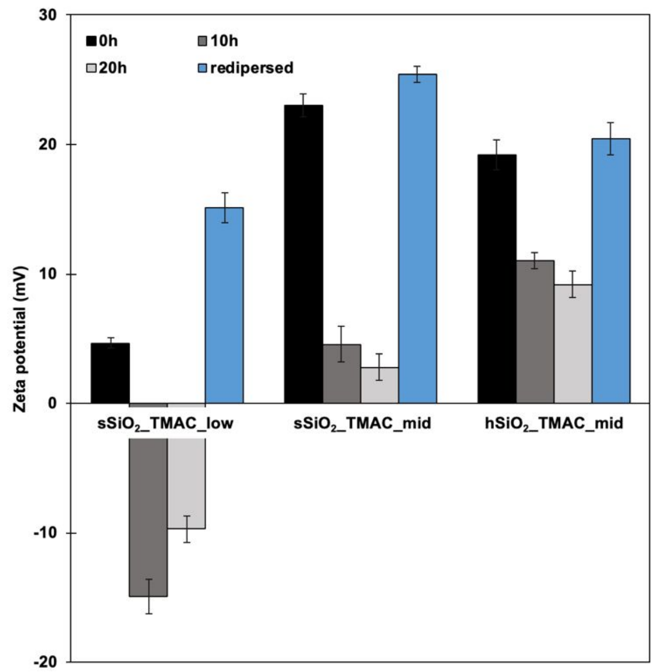

Figure 6. Zeta potentials of three different TMAC-modified silica nanoparticles incubated in water at concentrations of 0.5 mg/mL. After 20 hours of the incubation, all nanoparticles were centrifuged and redispersed in the same volume of water to removed released silicic acid in solution and adsorbed on the nanoparticles.

Taking one more step toward obtaining nanoparticles possessing and maintaining a stable positive zeta potential, chlorotrimethylsilane (TMS) was also added during the synthesis after TMAC addition. TMS has a small hydrophobic trimethyl group which has been proven to delay the hydrolysis of silica nanoparticle.[38] The nanoparticles after TMS modification were incubated in higher temperature (95 °C) as well, to expedite more complete hydrolysis of the inner regions and condensation on the shells. Figure 7 shows three positively charged hollow silica nanoparticle preparations before/after TMS addition and hydrothermal treatment. All nanoparticles showed more dense and thicker shells after the additional modification, mainly due to the TMS condensation on the surface. The $hSiO_2$_TMAC_high nanoparticles, which had incomplete hollow structures before the hydrothermal treatment, showed improved hollow character after the treatment.

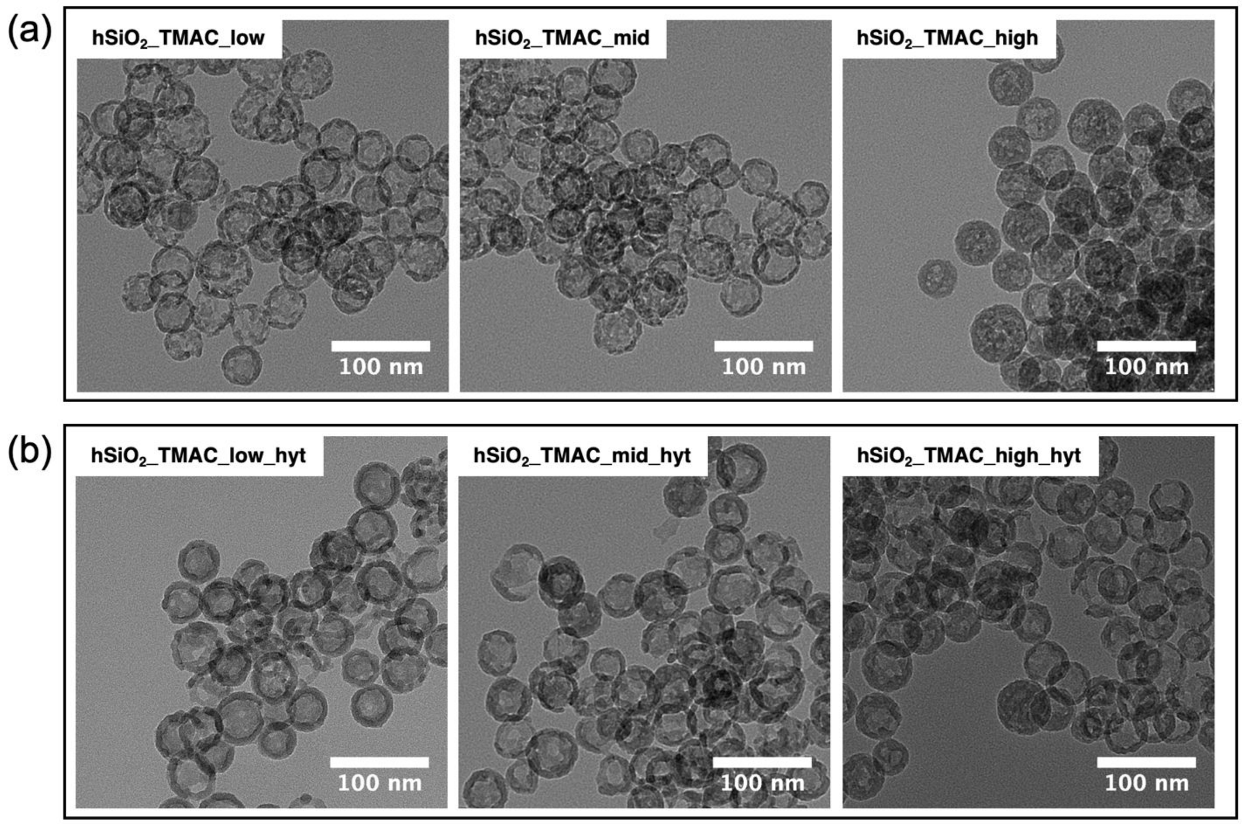

Figure 7. TEM images of silica nanoparticles (a) without hydrothermal treatment and TMS addition ($hSiO_2$_TMAC) and (b) with hydrothermal treatment and TMS addition ($hSiO_2$_TMAC_hyt). During the synthesis, the volumes of the diluted TMAC were varied to 20 μL, 100 μL, and 270 μL for low, mid, and high concentrations, respectively.

The effects of the two additional modifications during the synthesis on the zeta potential maintenance were evaluated, and all three nanoparticles showed more stable potential in water for 24 hours compared to non-TMS/hydrothermal treatment hollow nanoparticles (Figure 8a), and the $hSiO_2$_TMAC_hyt nanoparticles even showed improved consistent positive zeta potentials for 7 days (Figure 8b), which couldn't be achieved with solid silica nanoparticles. Clearly, the morphology, and the concordant extent of condensation, of the silica nanoparticles impacts the surface electric potential maintenance, especially when the silane used for surface modification has the opposite charge as common silanol groups.

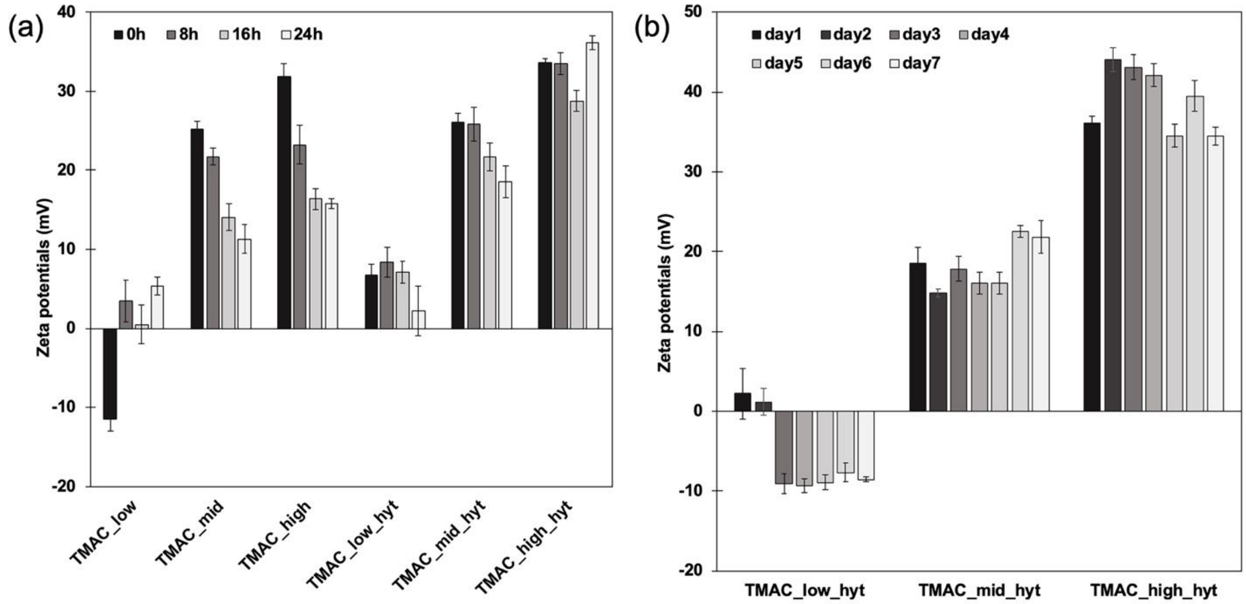

Figure 8. (a) Zeta potentials of TMAC-functionalized hollow silica without either TMS addition or hydrothermal treatment (no "hyt" in their labels) and with the TMS addition and the hydrothermal treatment (with "hyt" in their labels) for 24 hours of incubation in pure water. (b) Zeta potentials of TMAC-functionalized hollow silica with TMS addition and hydrothermal treatment for 7 days of incubation in water. The concentrations were 0.5 mg/mL for all samples.

Conclusion

In this work, quaternary ammonium silane-modified silica nanoparticles of around 45 nm in diameters were synthesized via reverse microemulsion to explore the impact of amorphous silica nanoparticle morphology on their electric potential maintenance in colloidal dispersion. The monodisperse silica with TMAC condensed on the surface was obtained when the nanoparticles were extracted from the emulsion and redispersed in solution for further silane condensation. In this case, even though TMAC was condensed on the surface of the nanoparticles with varying coverage to induce different positive potentials, nanoparticles showed time-dependent potential loss in aqueous colloidal suspension with the change in zeta potentials from > 40 mV to nearly 0 mV within 24 hours. It was concluded that this occurred not from the surface TMAC hydrolysis but from the adsorption of silicic acid dissolved from the inner regions where silica precursors exist with incomplete condensation. To mitigate the possibility of core region hydrolysis, the template solid silica was post-treated in basic solution with TMAC introduction, where the template nanoparticle dissolution from the cores and the TMAC condensation on the surface occur at the same time. With tuned concentrations of nanoparticles and TMAC, a hollow structure was achieved with a set of varied zeta potentials of approximately 5 mV, 20 mV, and > 30 mV in aqueous dispersion, and these hollow nanoparticles were further modified with a hydrophobic silane in a higher temperature to enhance their resistance against hydrolysis during aqueous suspension by showing much more improved consistent zeta potentials values for seven days of incubation. The hollow structure clearly showed improved positive zeta potential maintenance, making these nanoparticles excellent candidates for a variety of biological and biomedical applications.

Acknowledgement

This work was supported by National Science Foundation under the Center for Sustainable Nanotechnology (CSN), CHE-1503408. The CSN is part of the Centers for Chemical Innovation Program. Parts of this work were carried out in the Characterization Facility, University of Minnesota, which receives partial support from NSF through the MRSEC program.

References

(1) Ciriminna, R.; Fidalgo, A.; Pandarus, V.; Béland, F.; Ilharco, L. M.; Pagliaro, M. The Sol–Gel Route to Advanced Silica-Based Materials and Recent Applications. *Chem. Rev.* **2013**, *113* (8), 6592–6620.
(2) Pandarus, V.; Gingras, G.; Béland, F.; Ciriminna, R.; Pagliaro, M. Selective Hydrogenation of Vegetable Oils over Silia *Cat* Pd(0). *Org. Process Res. Dev.* **2012**, *16* (7), 1307–1311.
(3) Ciriminna, R.; Pagliaro, M. Tailoring the Catalytic Performance of Sol–Gel-Encapsulated Tetra-n-Propylammonium Perruthenate (TPAP) in Aerobic Oxidation of Alcohols. *Chem. - Eur. J.* **2003**, *9* (20), 5067–5073.
(4) Pagliaro, M.; Hutchings, G. J. Heterogeneous Catalysis for Fine Chemicals. *Catal. Sci. Technol.* **2011**, *1* (9), 1543.
(5) Wei, L.; Hu, N.; Zhang, Y. Synthesis of Polymer—Mesoporous Silica Nanocomposites. *Materials* **2010**, *3* (7), 4066–4079.
(6) Ilharco, L. M.; Fidalgo, A.; Farinha, J. P. S.; Martinho, J. M. G.; Rosa, M. E. Nanostructured Silica/Polymer Subcritical Aerogels. *J. Mater. Chem.* **2007**, *17* (21), 2195.
(7) Li, Z.; Barnes, J. C.; Bosoy, A.; Stoddart, J. F.; Zink, J. I. Mesoporous Silica Nanoparticles in Biomedical Applications. *Chem. Soc. Rev.* **2012**, *41* (7), 2590.
(8) Li, J.-F.; Zhang, Y.-J.; Ding, S.-Y.; Panneerselvam, R.; Tian, Z.-Q. Core–Shell Nanoparticle-Enhanced Raman Spectroscopy. *Chem. Rev.* **2017**, *117* (7), 5002–5069.
(9) Xie, M.; Shi, H.; Ma, K.; Shen, H.; Li, B.; Shen, S.; Wang, X.; Jin, Y. Hybrid Nanoparticles for Drug Delivery and Bioimaging: Mesoporous Silica Nanoparticles Functionalized with Carboxyl Groups and a near-Infrared Fluorescent Dye. *J. Colloid Interface Sci.* **2013**, *395*, 306–314.
(10) Manuchehrabadi, N.; Gao, Z.; Zhang, J.; Ring, H. L.; Shao, Q.; Liu, F.; McDermott, M.; Fok, A.; Rabin, Y.; Brockbank, K. G. M.; et al. Improved Tissue Cryopreservation Using Inductive Heating of Magnetic Nanoparticles. *Sci. Transl. Med.* **2017**, *9* (379), eaah4586.
(11) Hyde, E. D. E. R.; Seyfaee, A.; Neville, F.; Moreno-Atanasio, R. Colloidal Silica Particle Synthesis and Future Industrial Manufacturing Pathways: A Review. *Ind. Eng. Chem. Res.* **2016**, *55* (33), 8891–8913.
(12) Liberman, A.; Mendez, N.; Trogler, W. C.; Kummel, A. C. Synthesis and Surface Functionalization of Silica Nanoparticles for Nanomedicine. *Surf. Sci. Rep.* **2014**, *69* (2–3), 132–158.
(13) Sun, Y.; Sai, H.; von Stein, F.; Riccio, M.; Wiesner, U. Water-Based Synthesis of Ultrasmall PEGylated Gold–Silica Core–Shell Nanoparticles with Long-Term Stability. *Chem. Mater.* **2014**, *26* (18), 5201–5207.
(14) Li, G. L.; Wan, D.; Neoh, K. G.; Kang, E. T. Binary Polymer Brushes on Silica@Polymer Hybrid Nanospheres and Hollow Polymer Nanospheres by Combined Alkyne−Azide and Thiol−Ene Surface Click Reactions. *Macromolecules* **2010**, *43* (24), 10275–10282.
(15) Lee, C.-H.; Lo, L.-W.; Mou, C.-Y.; Yang, C.-S. Synthesis and Characterization of Positive-Charge Functionalized Mesoporous Silica Nanoparticles for Oral Drug

Delivery of an Anti-Inflammatory Drug. *Adv. Funct. Mater.* **2008**, *18* (20), 3283–3292.
(16) Shahabi, S.; Treccani, L.; Dringen, R.; Rezwan, K. Modulation of Silica Nanoparticle Uptake into Human Osteoblast Cells by Variation of the Ratio of Amino and Sulfonate Surface Groups: Effects of Serum. *ACS Appl. Mater. Interfaces* **2015**, *7* (25), 13821–13833.
(17) Shahabi, S.; Döscher, S.; Bollhorst, T.; Treccani, L.; Maas, M.; Dringen, R.; Rezwan, K. Enhancing Cellular Uptake and Doxorubicin Delivery of Mesoporous Silica Nanoparticles via Surface Functionalization: Effects of Serum. *ACS Appl. Mater. Interfaces* **2015**, *7* (48), 26880–26891.
(18) Zhao, J.; Wu, S.; Qin, J.; Shi, D.; Wang, Y. Electrical-Charge-Mediated Cancer Cell Targeting via Protein Corona-Decorated Superparamagnetic Nanoparticles in a Simulated Physiological Environment. *ACS Appl. Mater. Interfaces* **2018**, *10* (49), 41986–41998.
(19) Wang, J.; Xu, D.; Deng, T.; Li, Y.; Xue, L.; Yan, T.; Huang, D.; Deng, D. Self-Decomposable Mesoporous Doxorubicin@Silica Nanocomposites for Nuclear Targeted Chemo-Photodynamic Combination Therapy. *ACS Appl. Nano Mater.* **2018**, *1* (4), 1976–1984.
(20) Cao, L.; Zhou, Z.; Niu, S.; Cao, C.; Li, X.; Shan, Y.; Huang, Q. Positive-Charge Functionalized Mesoporous Silica Nanoparticles as Nanocarriers for Controlled 2,4-Dichlorophenoxy Acetic Acid Sodium Salt Release. *J. Agric. Food Chem.* **2018**, *66* (26), 6594–6603.
(21) Finnie, K. S.; Bartlett, J. R.; Barbé, C. J. A.; Kong, L. Formation of Silica Nanoparticles in Microemulsions. *Langmuir* **2007**, *23* (6), 3017–3024.
(22) Jung, H.-S.; Moon, D.-S.; Lee, J.-K. Quantitative Analysis and Efficient Surface Modification of Silica Nanoparticles. *J. Nanomater.* **2012**, *2012*, 1–8.
(23) Thanh, N. T. K.; Maclean, N.; Mahiddine, S. Mechanisms of Nucleation and Growth of Nanoparticles in Solution. *Chem. Rev.* **2014**, *114* (15), 7610–7630.
(24) Lin, C.-H.; Chang, J.-H.; Yeh, Y.-Q.; Wu, S.-H.; Liu, Y.-H.; Mou, C.-Y. Formation of Hollow Silica Nanospheres by Reverse Microemulsion. *Nanoscale* **2015**, *7* (21), 9614–9626.
(25) Yu, Q.; Wang, P.; Hu, S.; Hui, J.; Zhuang, J.; Wang, X. Hydrothermal Synthesis of Hollow Silica Spheres under Acidic Conditions. *Langmuir* **2011**, *27* (11), 7185–7191.
(26) Zhang, T.; Zhang, Q.; Ge, J.; Goebl, J.; Sun, M.; Yan, Y.; Liu, Y.; Chang, C.; Guo, J.; Yin, Y. A Self-Templated Route to Hollow Silica Microspheres. *J. Phys. Chem. C* **2009**, *113* (8), 3168–3175.
(27) Chen, Y.; Chen, H.; Guo, L.; He, Q.; Chen, F.; Zhou, J.; Feng, J.; Shi, J. Hollow/Rattle-Type Mesoporous Nanostructures by a Structural Difference-Based Selective Etching Strategy. *ACS Nano* **2010**, *4* (1), 529–539.
(28) Hu, H.; Zhou, H.; Liang, J.; An, L.; Dai, A.; Li, X.; Yang, H.; Yang, S.; Wu, H. Facile Synthesis of Amino-Functionalized Hollow Silica Microspheres and Their Potential Application for Ultrasound Imaging. *J. Colloid Interface Sci.* **2011**, *358* (2), 392–398.

(29) Nandiyanto, A. B. D.; Akane, Y.; Ogi, T.; Okuyama, K. Mesopore-Free Hollow Silica Particles with Controllable Diameter and Shell Thickness via Additive-Free Synthesis. *Langmuir* **2012**, *28* (23), 8616–8624.
(30) Metin, C. O.; Baran, J. R.; Nguyen, Q. P. Adsorption of Surface Functionalized Silica Nanoparticles onto Mineral Surfaces and Decane/Water Interface. *J. Nanoparticle Res.* **2012**, *14* (11).
(31) Danks, A. E.; Hall, S. R.; Schnepp, Z. The Evolution of 'Sol–Gel' Chemistry as a Technique for Materials Synthesis. *Mater. Horiz.* **2016**, *3* (2), 91–112.
(32) Alexander, G. B.; Heston, W. M.; Iler, R. K. The Solubility of Amorphous Silica in Water. *J. Phys. Chem.* **1954**, *58* (6), 453–455.
(33) Crundwell, F. K. On the Mechanism of the Dissolution of Quartz and Silica in Aqueous Solutions. *ACS Omega* **2017**, *2* (3), 1116–1127.
(34) Kajihara, K. Recent Advances in Sol–Gel Synthesis of Monolithic Silica and Silica-Based Glasses. *J. Asian Ceram. Soc.* **2013**, *1* (2), 121–133.
(35) Wong, Y. J.; Zhu, L.; Teo, W. S.; Tan, Y. W.; Yang, Y.; Wang, C.; Chen, H. Revisiting the Stöber Method: Inhomogeneity in Silica Shells. *J. Am. Chem. Soc.* **2011**, *133* (30), 11422–11425.
(36) Teng, Z.; Su, X.; Zheng, Y.; Sun, J.; Chen, G.; Tian, C.; Wang, J.; Li, H.; Zhao, Y.; Lu, G. Mesoporous Silica Hollow Spheres with Ordered Radial Mesochannels by a Spontaneous Self-Transformation Approach. *Chem. Mater.* **2013**, *25* (1), 98–105.
(37) Zhang, Q.; Zhang, T.; Ge, J.; Yin, Y. Permeable Silica Shell through Surface-Protected Etching. *Nano Lett.* **2008**, *8* (9), 2867–2871.
(38) Lin, Y.-S.; Abadeer, N.; Hurley, K. R.; Haynes, C. L. Ultrastable, Redispersible, Small, and Highly Organomodified Mesoporous Silica Nanotherapeutics. *J. Am. Chem. Soc.* **2011**, *133* (50), 20444–20457.

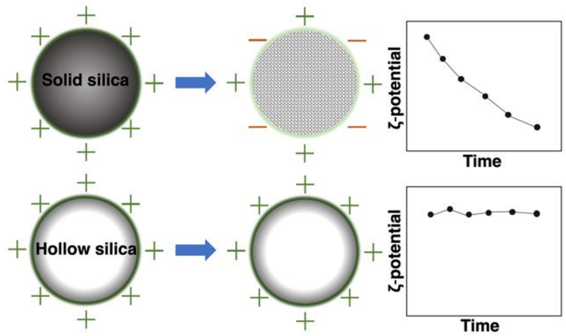

Table of Contents